Novel approach to copper sintering using surface enhanced brass micro flakes for microelectronics packaging

Sri Krishna Bhogaraju[1*], Fosca Conti[2*], Hiren R. Kotadia[3], Simon Keim[4], Ulrich Tetzlaff[4], Gordon Elger[1]

[1] Institute of Innovative Mobility, Technische Hochschule Ingolstadt, Esplanade 10, 85049, Ingolstadt, Germany.

[2] Department of Chemical Sciences, University of Padova, Via Marzolo 1, 35131, Padova, Italy.

[3] Warwick Manufacturing Group (WMG), The University of Warwick, CV47AL, United Kingdom.

[4] Technische Hochschule Ingolstadt, Esplanade 10, 85049, Ingolstadt, Germany.

[*] Corresponding authors – srikrishna.bhogaraju@thi.de, fosca.conti@unipd.it

Abstract

Copper pastes suitable for low temperature and low pressure die-attach bonding were developed to enable sintering at 275 °C under N_2 atmosphere. First, brass flakes were treated with HCl to selectively etch Zn and to realize enhanced surface modifications on the flakes. Then, polyethylene glycol was added as binder to the modified flakes due to its reducing effects on copper oxides and its property to prevent agglomeration. Shear strength of ca. 50 MPa was achieved while sintering with 10 MPa bonding pressure thereby providing suitable, easy and low-cost sintering pastes for microelectronics packaging applications.

Keywords

Metals and alloys, microstructure, surfaces and interfaces, sintering

1. Introduction

Restrictions on the use of hazardous materials and rapid progresses in the field of electric vehicles are among the major contributing factors towards the development of alternatives to high Pb solders which are capable of ensuring reliable operation for high temperature (> 175 °C) microelectronics packaging applications [1,2]. Ag sintering has been a major focus of research over the past decade as a solution to Pb-free soldering [3]. However, reported susceptibility of Ag sintered interconnects to electromigration [4] and high cost of Ag are motivating factors to investigate alternatives. Cu offers the advantage of comparable electrical and mechanical properties to Ag at a fraction of the cost. Cu is more resistant to electromigration, abundantly available and easily recyclable, thereby offering a sustainable alternative. However, a major challenge is the high affinity of Cu to oxidize, a spontaneous reaction, thermodynamically and kinetically favourable by increasing temperature [5,6]. In addition, the higher melting point of Cu (1085 °C) would mean a higher sintering temperature compared to Ag, when working with particles of comparable morphologies. Solutions to tackle these challenges in Cu sintering range mainly from using reducing atmosphere (H_2 or formic acid enriched N_2) during sintering [7–10], using reducing binders in pastes [11,12], oxidation-reduction bonding processes [13], Cu core shell particles with Ag/Sn outer layers [14,15] and phosphating Cu nanoparticles [16]. While these solutions are promising at laboratory scale experiments, the high sintering temperatures (> 300 °C) and the intensive and expensive process of development of Cu nanoparticles are challenges in upscaling to real-world applications. Recently, Cu salts were investigated as promising interconnect material for die-attach bonding [17] However, the price of Cu salts is a relevant aspect in the cost-benefit analysis of many applications. Cu and brass flakes are ca. 5 times less expensive than Cu salts and can be commercially procured for less than 100 $/Kg. In this paper, an easy and low-cost solution using surface enhanced Cu and brass flakes is introduced. To improve the sinterability of the flakes, high surface roughness and morphological modifications are realized through a wet chemical etching process. After etching, the flakes are dispersed in polyethylene glycol 600 (PEG600) which is reported to be successful in reducing copper oxides [17]. The combination between the thin flake morphology of the materials with enhanced surface modifications and the reducing binder allows for sintering at 275 °C in N_2 atmosphere. Under the application of a bonding pressure of 10 MPa, shear strength of ca. 50 MPa was achieved which is considerably higher than the requirements specified under the test method standard for microcircuits (MIL-STD-883E) [18].

2. Materials, samples preparation and characterization

Cu and brass flakes with a thickness of ca. 200 nm and a diameter of approximately 3-5 µm were sourced by Schlenk Metallic Pigments GmbH, Germany. Three different brass flakes were investigated, with compositions between 2.5 and 25.7 wt% of Zn (**Error! Reference source not found.**1). For wet chemical etching, 100 g of flakes were stirred in 600 ml of 12M HCl at 600 rpm for 4 hours at room temperature. The flake concentration in acid was chosen to ensure efficient stirring, thereby avoiding coagulation of the flakes during etching. A scanning electron microscope (SEM) was used for the analysis of the flakes before and after etching and for the corresponding microstructure evaluation. Characterization of the flakes by X-ray diffraction spectrometry (XRD) was carried out using a Panalytical Empyrean diffractometer with Co-Kα1 radiation (λ= 1.788 Å) at an accelerating voltage of 40 kV. The XRD was collected with a step size of 0.03° over the angular range 30–100° (2θ) with a total collection time of 58 min. The XRD patterns of the flakes before etching and after etching were analysed and compared using the Panalytical HighScore Plus software package, containing the 2016 database. PEG600 was used as binder for the formulation of the pastes. The developed pastes were intended to satisfy the requirements of stencil printing, which is a standard technology in die-attach bonding. The pastes (i) can be easily printed through the stencil apertures, (ii) do not stick to the squeeze or clump on the stencil, and (iii) hold their shape after printing. Different weight ratios of etched flakes to binder were investigated. The weight ratio of 63/37 was determined as optimal. This ratio was selected based on the best results of printability of the pastes in terms of consistency, adherence, stickiness, and compressibility. An excessive amount of binder led to a spread out at the edges and corners during the printing process. On the contrary, with PEG600 lesser than 37 wt%, a consistent print was not enabled. Mixing of the paste was performed in a planetary rotary mixer for 4 min at 1000 rpm followed by 5 min at 500 rpm. A PBT-Uniprint-PMGo3v semi-automatic stencil printer equipped with a motorized double blade squeegee and a 75 µm thick stencil was used. Sintering was performed under the application of 10 MPa bonding pressure at 275 °C for 30 min under N_2 atmosphere with a ramp rate of 1 K/s. Si_3N_4 chips (1.55 x 1.6 x 0.08 mm^3) with Pt/Au metallization were used as test chips and Cu substrates (12x12x1mm^3) with electroless Ni immersion Au (ENIG) metallization were used as substrates. The chip was placed on the printed paste only after the sintering temperature was reached to ensure sufficient degassing of the binder. Shear tests were performed on a XYZ-Condor Sigma Lite shear tester under a shear speed of 25 µm/s. Finally, the porosity of the sintered interconnects was calculated using open source image processing program ImageJ.

3. Results and discussions

Equations 1-3 describes the chemical reactions occurring in the etching process: Selective etching of Zn from the brass flakes (equation 1) and etching of Cu oxides from the Cu flakes (equation 2 and 3). Because of the reduction potentials, Cu does not react with HCl. After etching, the flakes were thoroughly rinsed first in distilled water and then in isopropanol to remove any traces of chlorine. $ZnCl_2$ and $CuCl_2$ are highly soluble in water with a solubility of 432g/100ml and 70.6g/100ml, respectively. CuCl is sparingly soluble in water (0.0062g/100ml), however highly soluble in concentrated HCl.

$$Zn_{(s)} + 2HCl_{(l)} \rightarrow ZnCl_{2\,(l)} + H_{2\,(g)} \quad (1)$$

$$CuO_{(s)} + 2HCl_{(l)} \rightarrow CuCl_{2\,(l)} + H_2O_{(l)} \quad (2)$$

$$Cu_2O_{(s)} + 2HCl_{(l)} \rightarrow 2CuCl_{(l)} + H_2O_{(l)} \quad (3)$$

Table 1 - Materials composition resulting from EDX element analysis and average shear strength across 5 measurements.

Sample name	Pristine Material	Zn (wt%) after etching	Zn lost (wt%)	Shear strength (MPa) after sintering
S1	Cu flakes	na	na	62 ± 3
S2	Brass flakes with 2.5 wt% Zn	0.7	72	56 ± 3
S3	Brass flakes with 7.7 wt% Zn	3.0	61	57 ± 2
S4	Brass flakes with 25.7 wt% Zn	6.4	75	46 ± 3

SEM analysis reveals the surface modifications on the flakes due to the etching (Fig. 1). The etching has the advantage to selectively etch Zn, thereby creating enhanced surface modifications on the brass flakes resulting in a favourable material morphology for low temperature and low pressure sintering [19]. The modifications are observed to be mainly increased curvatures and edges along the surfaces of the flakes, giving them a rough texture as compared to the original flakes, which show a smooth surface. These are extensively reported as contributing factors in enhancing sinterability of metal particles at low temperatures [20,21] All starting materials had a Zn content less than 30 wt%, with the indication of α-brass phase.

In α-brass, Zn is completely dissolved in the Cu, forming a solid solution [22]. Table 1 shows the percentage drop of Zn after etching. Because all starting materials have the same size, no correlations with the flake dimensions are investigated. XRD analysis of the particles before and after etching is shown in Fig. 2. Pure Cu flakes (Fig. 2a-b) and brass flakes (Fig. 2c-f) reveal the typical three major Cu peaks and Zn peaks in all the brass samples. As expected, low intensity Cu oxide peaks due to CuO and Cu_2O are also detected in the starting materials. After etching, CuCl was detected for brass flakes S2 (Fig. 2d) indicating inadequate cleaning. In case of brass flakes S4, Cu0.7Zn0.3 phases are identified in the original flakes. Similar phases have been earlier reported in the CuZn system consisting of up to 30 wt% of Zn [23,24]. However, after etching new pure Cu peaks appear and the Cu0.7Zn0.3 phase can be identified along the shoulder of the newly developed pure Cu peaks.

In the case of Cu flakes S1, after etching and drying in ambient atmosphere for 24 hours, tiny mound-like structures are observed on the surfaces (Fig. 1b). These features can be identified as Cu_2O nanoparticles by the more pronounced Cu_2O peaks observed in the XRD analysis of the etched flakes. The etching compromises the protective layer formed on the flakes by stearic acid used during the ball milling process, thereby exposing the Cu particles to oxidation during the drying process. The structures seen are consistent with observations reported in literature on the oxidation of reduced Cu nanoparticles [25]. Similar features have been earlier reported to enhance sintering during the oxidation-reduction bonding process of Cu particles after their oxidation in air [13]. In case of brass, the surface modifications are due to the selective etching of Zn from the alloy and therefore a rough surface texture is created. With residual Zn still left in the flakes and acting as a sacrificial anode, no pronounced Cu_2O peaks are observed like in the case of Cu flakes [26,27].

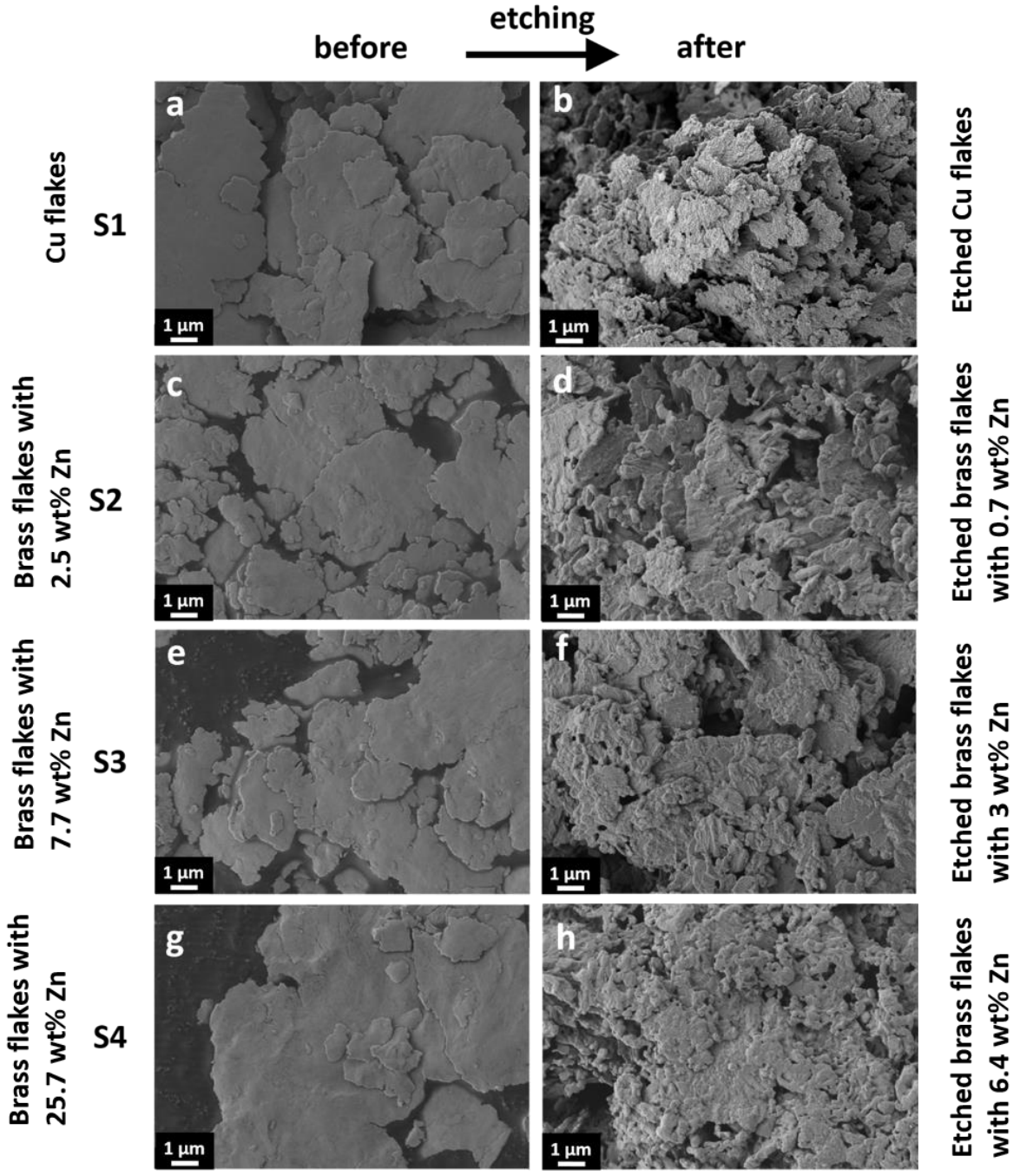

Fig. 1 - SEM images of the flakes before (a, c, e, g) and after (b, d, f, h) etching for 4 hours in 12 M HCl showing enhances surface modifications on the flakes.

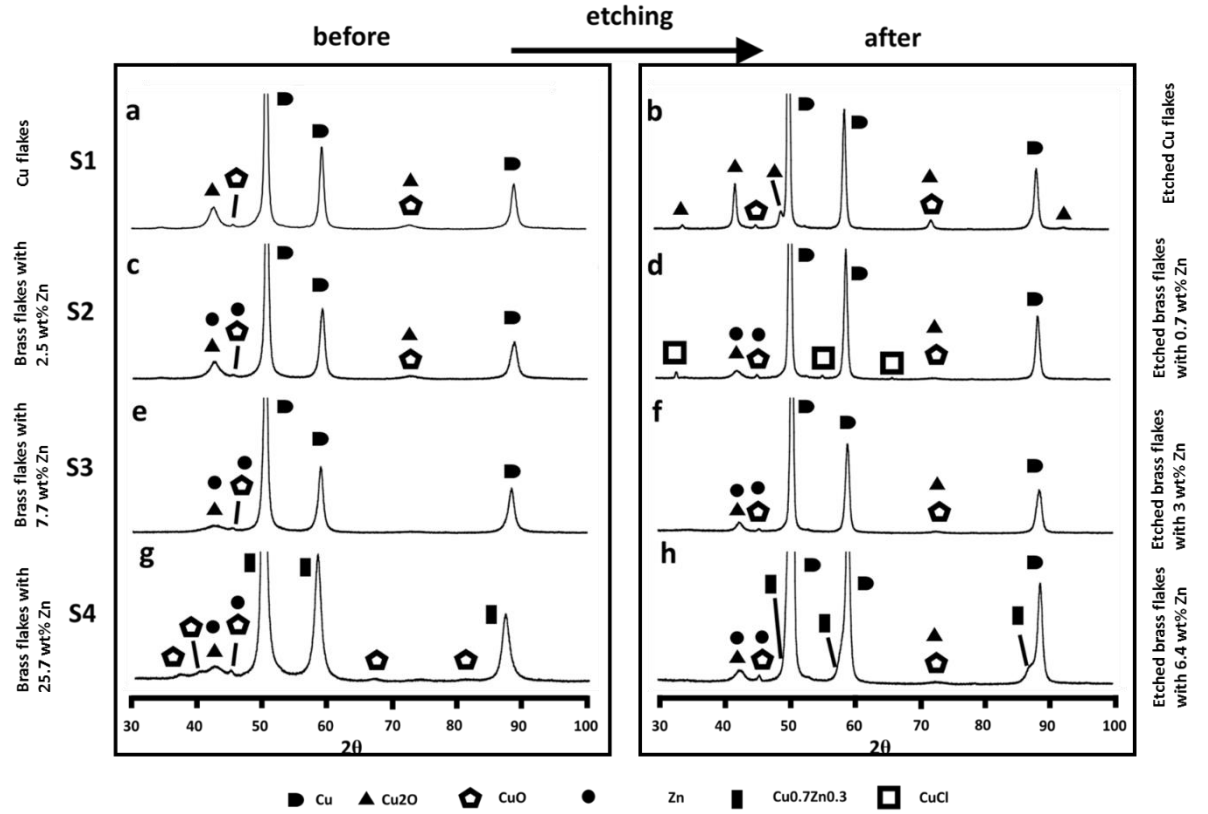

Fig. 2 - XRD analysis of the flakes before (a, c, e, g) and after (b, d, f, h) etching in 12M HCl for 4 hours at room temperature.

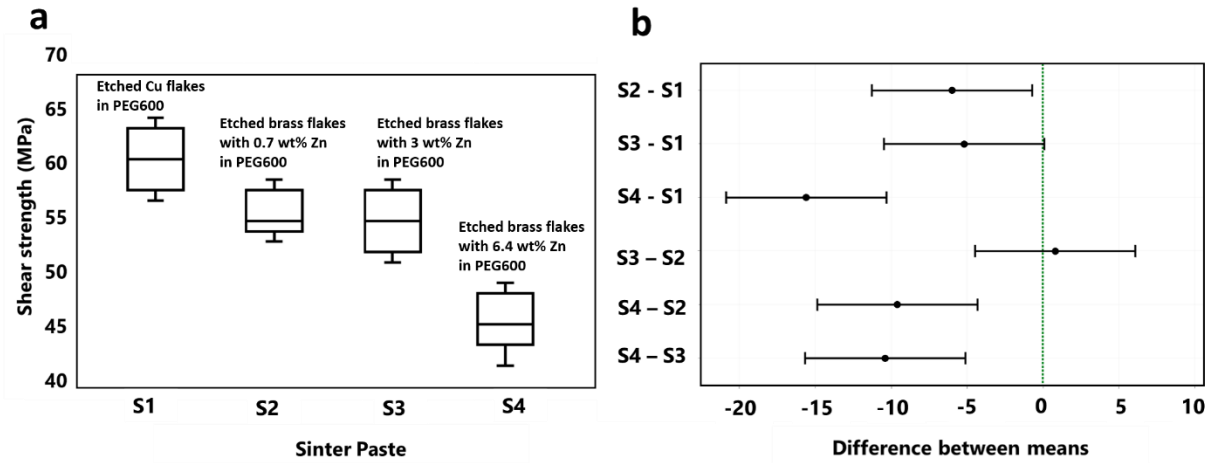

Fig. 3 – Analysis of shear strength values among all interconnections made by the four pastes with PEG600 as binder: (a) Box plot and (b) Tukey-Kramer method of pairwise comparison (equivalent to 95% simultaneous confidence level).

Based on the sintering process developed with the application of 10 MPa bonding pressure at 275 °C for 30 min in N_2 atmosphere, the sintering characteristics of the four interconnects were compared. Table 1 lists the shear strength values of the interconnects which were realized by sintering with each of the four developed pastes. Boxplots in Fig. 3a graphically depict the groups of values though their quartiles. To analyse the shear strength values, the Tukey-Kramer

method was applied with a significance level of 0.05. A single-step procedure for pairwise comparisons among all samples was used to identify which specific groups had significantly different means from one another. The results of Fig. 3b indicate that the means for the pair S3–S2 are not significantly different, for the pair S3-S1 are only marginally different while for the rest the means are significantly different from each other.

Surface diffusion is a major contributing factor towards the development of necks between particles at low sintering temperatures [21,28]. Working with surface modified flakes offers an advantage because flakes have a high free surface energy due to their large specific surface area compared to spherical particles of the same size. With Ag sintering, better necking behaviour was observed while working with Ag flakes as compared to spherical Ag particles [29]. SEM analyses of the cross sections of the interconnection (Fig. 4) reveal homogeneous microstructures between the flakes in all the realized assemblies. In case of paste-S1, obtained with etched Cu flakes in PEG600, a bulk like interconnect is observed. This paste also returned the best shear strength value (62 ± 3 MPa) among the others (between 46 and 57 MPa). Cu oxides on the flakes are a hindrance to surface diffusion during sintering as they are thermodynamically more stable than pure Cu and increase the sintering temperature [30]. The disadvantages of oxidation of Cu particles and the consequent hindrance to sinterability, both between particles as well as to the substrate are eliminated by the use of PEG600, which is demonstrated to be effective in reducing Cu oxides [31]. The use of the PEG600 in the paste formulation enables the *in-situ* reduction of Cu oxides during the sintering process. The reduction products are Cu nanoparticles which act as nano joiners between the µ-sized flakes thereby realising a bulk like microstructure with higher shear strength in case of the etched Cu flakes. In case of paste-S4 (Fig. 4d), it returned the lowest shear strength (46 ± 3 MPa).

Porosity of the microstructure affects the mechanical and thermal integrity of the interconnect. It is mainly related to sintering parameters (e.g. time, pressure, temperature, heating rate, atmosphere) [20] and paste formulation (e.g. physical-chemical properties of the materials, grain geometry and size, interaction between particles and binder). Under the sintering conditions of the present study (275 °C, 10 MPa, 30 min, N_2 atmosphere), the four developed pastes have appropriate high shear strength but different types of microstructure and porosity. This could be beneficial for specific applications: for example, a sponge-like porous microstructure with homogeneous distributed pores will be beneficial for applications where stress relaxation after sintering is required, i.e. when joining materials with large thermo-mechanical mismatch. The porous microstructure with small homogeneous distributed pores

targets in addition the reduction of crack propagation in the interconnect and by that a high thermo-mechanical fatigue resistance.

The sintering characteristics of the four interconnects were compared in terms of porosity, and average pore size and distribution. Image analysis of the representative SEM images of the cross sections provides an indication of the area fraction of the porosity across the particular plane for each of the characterized specimen as shown in Fig 4(a1-d1). Paste-S1 (~6% porosity) shows isolated pores with average pore area of 0.03μm² (n = 1021) while pastes-S2 (~19% porosity), -S3 (~21% porosity) reveal homogeneous interconnect with sponge-like porous matrix with average pore area of 0.12 μm² (n = 1021) and 0.11 μm² (n = 1102) respectively. Paste-S4 (~26% porosity) shows finely distributed interconnected pores with average pore area of 0.04μm² (n = 4354) with 'n' denoting the total number of pores. The pore share factor (F) is reported to provide an indication on the microstructure evolution [32]. It is calculated by using the formula:

$$F = (4\pi A)/P^2 \qquad (4)$$

where A is the pore area and P is the perimeter of the pore. The analysis reveals that a majority of the pores in the sintered interconnects of paste-S1 are in the range of near spherical to spherical shaped pores ($F \geq 0.8$) while in case of paste-S2, -S3 and -S4 predominantly irregular shaped pores are observed ($F < 0.7$). This is also evident from the microstructure of the sintered interconnect shown in Fig. 4 which shows isolated pores in case of past-S1 and interconnected pores in case of -S2, -S3 and -S4. The average area of the pores in paste-S2 and -S3 is ~ factor 3 larger than in case of -S1 and -S4 which are dominated by pores < 0.2 μm². However, excellent necking between the particles is observed in the sintered interconnects of paste-S2 and -S3 and bulk like sintering in -S1 which explains the high shear strength compared to -S4. The enhanced densification in case of -S1 as compared to the other pastes under the same bonding conditions is attributed to the *in-situ* formation of Cu nanoparticles, i.e. the reduction of Cu_2O particles to Cu nanoparticles, under the action of PEG600. In comparison to microparticles, nanoparticles are observed to sinter better together even under pressurelesss conditions [17] and reported to enhance sintering densification in case of Ag sinter sinter pastes [33–35]. The application of bonding pressure of 10MPa contributes further in achieving a densely packed structure. In case of the interconnect of paste-S4, although the average pore area and size are similar to paste-S1 and substantially smaller compared to -S2 and -S3, the pore distribution shows that the number of pores is a factor ~4 higher than that in the other samples indicating a large number of small pores distributed across the sintered interconnect (Fig. 4d1). The SEM analysis of the interconnect reveals clustered sintering between the particles with insufficient necking (Error!

Reference source not found.) and high porosity (ca. 26%, Fig. 4d1). These two observed phenomena are the most probable factors for the lower shear strength values of paste S-4. Further, the residual Zn in the microstructure as well as the Cu0.7Zn0.3 phase as identified by the XRD analysis could also be reasons for the lower mechanical integrity of the interconnect [36].

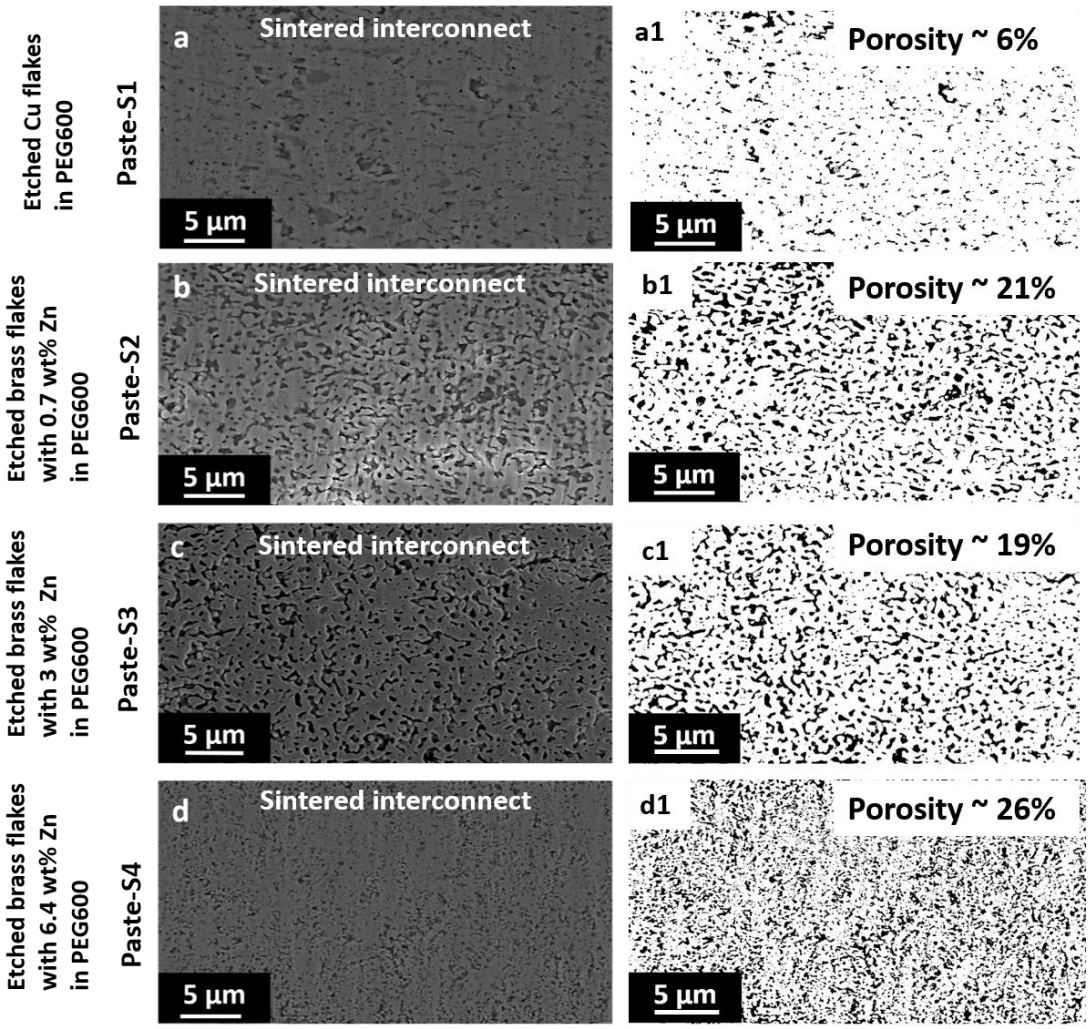

Fig. 4 – SEM images of the cross-section of the sintered interconnects. a1-d1: Grayscale images with the measured porosity values calculated across the cross-sections.

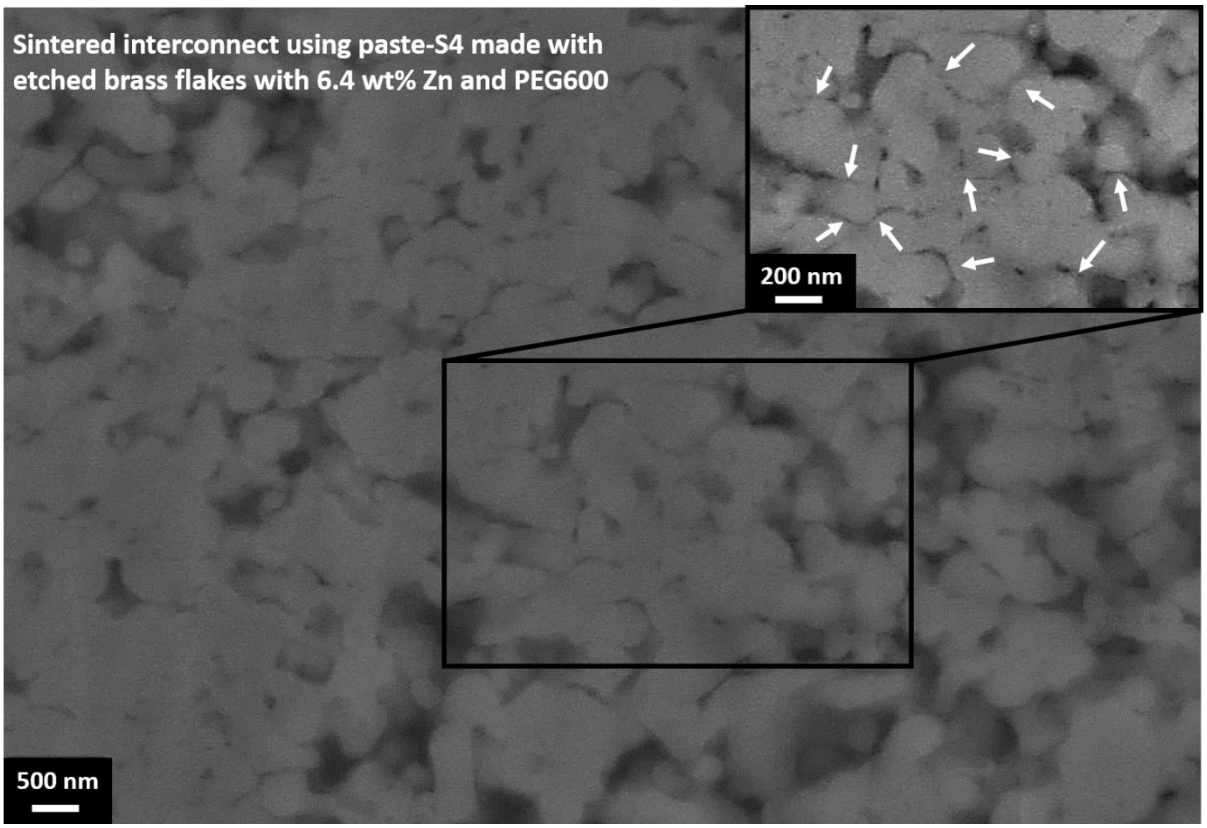

Fig. 5 - SEM images of the cross section of the sintered interconnect obtained using paste-S4 made by etched brass flakes with 6.4 wt% Zn and PEG600. Arrows in 200 nm scale image highlight insufficient necking between the particles.

Interfacial processes are crucial in many applications and are required to assure efficient thermal and electrical conductivity between the components. Indeed, insufficient bonding at the interfaces drastically affects the performance and long term reliability of the assembly as it can be a source of delaminations during the active lifecycle. Fig. 6 shows the interface regions characterizing the Si_3N_4 chip/sintered interconnect/Cu assemblies. All four investigated pastes show good sinterability to the substrate and chip metallization. In all assemblies, the sintering at the interface reflects the morphology of the microstructure observed in the interconnect bulk. Analysis of the interconnects after shear testing provides a good overview of the nature of the fracture. In all cases, after shear testing, the fracture was always in the interconnect bulk which confirms a strong bonding at the interface.

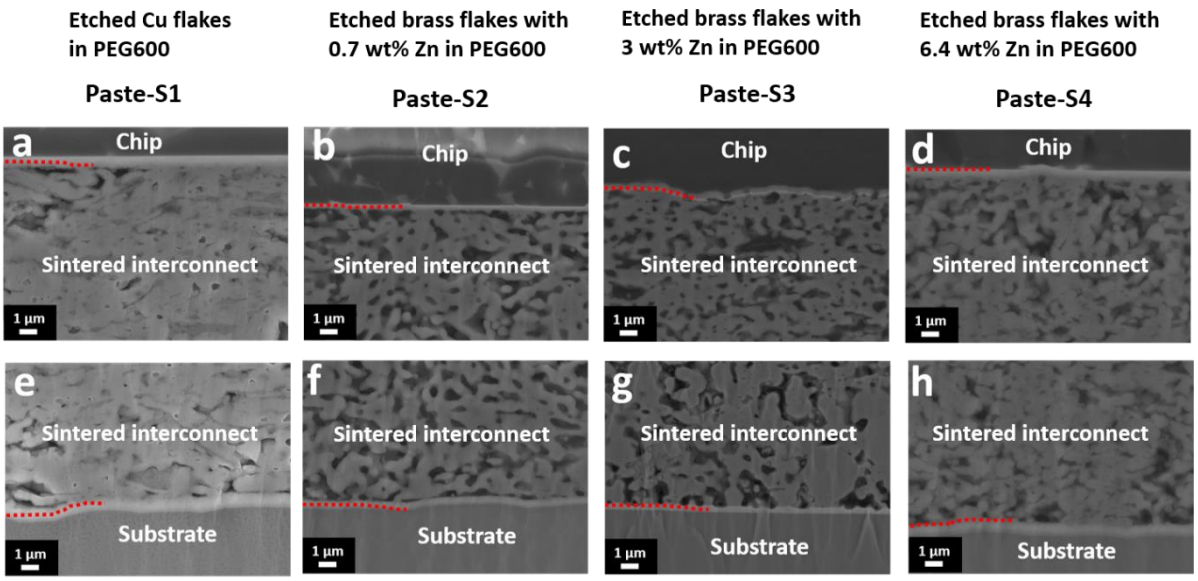

Fig. 6 – SEM cross-section images of sinterability to the ENIG substrate and to the Pt/Au Si_3N_4 chip metallization while sintering under 10 MPa bonding pressure at 275 °C for 30 min in nitrogen atmosphere. Red dotted lines indicate the interface between sintered interconnect and chip or substrate.

4. Conclusions

Cu pastes for die-attach applications were prepared with a novel easy and low-cost approach based on the realization of surface modifications on Cu and brass flakes by etching with HCl. While the surface modifications led to enhanced sinterability of the flakes, the thin flakes type morphology allowed for the formation of a dense and close packing structure even under the application of a low bonding pressure. The pastes could be sintered at 275 °C and under N_2 atmosphere due to the use of PEG600 in the formulation of the paste. The approach offers a promising alternative to existing die-attach bonding processes for ENIG copper and Pt/Au metallisation. Finally, the observed morphological evolution of the microstructure under the same bonding conditions in the developed pastes, ranging from a dense bulk-like to a sponge-like microstructure allows for the use of the pastes in a wide range of applications. In future, experiments to determine the correlations between pore size and grain size of the different materials, and the impact of the bonding parameters on the mechanical properties, i.e. thermo mechanical fatigue and creep, of the sintered interconnect and compatibility to other standard metallizations will be investigated.

Acknowledgements

This research was funded by the German Federal Ministry of Education and Research within the projects ProLoMa 13FH147PX6 and IQLED 13FH044PX8 under the program “Forschung an Fachhochschulen mit Unternehmen (FHprofUnt)”.

References

[1] C.C. Lee, C.-H. Sha, Y.-Y. Wu, S.-J. Hsu, Advanced Bonding/Joining Techniques, in: Mater. Adv. Packag., Springer International Publishing, Cham, 2017: pp. 27–90. https://doi.org/10.1007/978-3-319-45098-8_2.

[2] Y. Gao, H. Zhang, W. Li, J. Jiu, S. Nagao, T. Sugahara, K. Suganuma, Die Bonding Performance Using Bimodal Cu Particle Paste Under Different Sintering Atmospheres, J. Electron. Mater. 46 (2017) 4575–4581. https://doi.org/10.1007/s11664-017-5464-2.

[3] C. Weber, M. Hutter, Ag sintering – An alternative large area joining technology, in: 2018 7th Electron. Syst. Technol. Conf., IEEE, 2018: pp. 1–8. https://doi.org/10.1109/ESTC.2018.8546503.

[4] K.S. Siow, Are Sintered Silver Joints Ready for Use as Interconnect Material in Microelectronic Packaging?, J. Electron. Mater. 43 (2014) 947–961. https://doi.org/10.1007/s11664-013-2967-3.

[5] A. Hanss, M. Schmid, S.K. Bhogaraju, F. Conti, G. Elger, Process development and reliability of sintered high power chip size packages and flip chip LEDs, in: 2018 Int. Conf. Electron. Packag. IMAPS All Asia Conf., IEEE, 2018: pp. 479–484. https://doi.org/10.23919/ICEP.2018.8374351.

[6] S.K. Bhogaraju, A. Hans, M. Schmid, G. Elger, F. Conti, Evaluation of silver and copper sintering of first level interconnects for high power LEDs, in: 2018 7th Electron. Syst. Technol. Conf., IEEE, 2018: pp. 1–8. https://doi.org/10.1109/ESTC.2018.8546499.

[7] Y. Rosen, R. Marrach, V. Gutkin, S. Magdassi, Thin Copper Flakes for Conductive Inks Prepared by Decomposition of Copper Formate and Ultrafine Wet Milling, Adv. Mater. Technol. 4 (2019) 1800426. https://doi.org/10.1002/admt.201800426.

[8] T. Yao, T. Matsuda, T. Sano, C. Morikawa, A. Ohbuchi, H. Yashiro, A. Hirose, In Situ Study of Reduction Process of CuO Paste and Its Effect on Bondability of Cu-to-Cu Joints, J. Electron. Mater. 47 (2018) 2193–2197. https://doi.org/10.1007/s11664-017-

6049-9.

[9] K. Schnabl, L. Wentlent, K. Mootoo, S. Khasawneh, A.A. Zinn, J. Beddow, E. Hauptfleisch, D. Blass, P. Borgesen, Nanocopper Based Solder-Free Electronic Assembly, J. Electron. Mater. 43 (2014) 4515–4521. https://doi.org/10.1007/s11664-014-3478-6.

[10] T. Fujimoto, T. Ogura, T. Sano, M. Takahashi, A. Hirose, Joining of pure copper using Cu nanoparticles derived from CuO paste, Mater. Trans. 56 (2015) 992–996. https://doi.org/10.2320/matertrans.MI201410.

[11] Y. Mou, J. Liu, H. Cheng, Y. Peng, M. Chen, Facile Preparation of Self-Reducible Cu Nanoparticle Paste for Low Temperature Cu-Cu Bonding, JOM. 71 (2019) 3076–3083. https://doi.org/10.1007/s11837-019-03517-5.

[12] J. Li, Q. Liang, C. Chen, T. Shi, G. Liao, Z. Tang, Cu-Cu Bonding by Low-Temperature Sintering of Self-Healable Cu Nanoparticles, in: 2019 IEEE 69th Electron. Components Technol. Conf., IEEE, 2019: pp. 661–666. https://doi.org/10.1109/ECTC.2019.00105.

[13] X. Liu, H. Nishikawa, Low-pressure Cu-Cu bonding using in-situ surface-modified microscale Cu particles for power device packaging, Scr. Mater. 120 (2016) 80–84. https://doi.org/10.1016/j.scriptamat.2016.04.018.

[14] Y. Tian, Z. Jiang, C. Wang, S. Ding, J. Wen, Z. Liu, C. Wang, Sintering mechanism of the Cu–Ag core–shell nanoparticle paste at low temperature in ambient air, RSC Adv. 6 (2016) 91783–91790. https://doi.org/10.1039/C6RA16474A.

[15] H. Nishikawa, X. Liu, S. He, Effect of bonding conditions on shear strength of joints at 200 °C using Sn-coated Cu particle, in: 2017 21st Eur. Microelectron. Packag. Conf. Exhib., IEEE, 2017: pp. 1–4. https://doi.org/10.23919/EMPC.2017.8346890.

[16] Y. Zuo, J. Shen, Y. Hu, R. Gao, Improvement of oxidation resistance and bonding strength of Cu nanoparticles solder joints of Cu–Cu bonding by phosphating the nanoparticle, J. Mater. Process. Technol. 253 (2018) 27–33. https://doi.org/10.1016/j.jmatprotec.2017.11.001.

[17] S.K. Bhogaraju, O. Mokhtari, F. Conti, G. Elger, Die-attach bonding for high temperature applications using thermal decomposition of copper (II) formate with polyethylene glycol, Scr. Mater. 182 (2020) 74–80. https://doi.org/10.1016/j.scriptamat.2020.02.045.

[18] Department of Defense, MIL-STD-883E Test Method Standard - Microcicrcuits, Method 1014.9, March 14, 1995.

[19] S.K. Bhogaraju, O. Mokhtari, J. Pascucci, A. Hanss, M. Schmid, F. Conti, G. Elger, Hybrid Cu particle paste with surface-modified particles for high temperature electronics packaging, in: 2019 22nd Eur. Microelectron. Packag. Conf. Exhib., IEEE, 2019: pp. 1–8. https://doi.org/10.23919/EMPC44848.2019.8951887.

[20] S.-J. Kang, Sintering: densification, grain growth and microstructure, 2004.

[21] G.C. Kuczynski, Self-Diffusion in Sintering of Metallic Particles, in: Sinter. Key Pap., Springer Netherlands, Dordrecht, 1990: pp. 509–527. https://doi.org/10.1007/978-94-009-0741-6_33.

[22] M. Kowalski, P.J. Spencer, Thermodynamic reevaluation of the Cu-Zn system, J. Phase Equilibria. 14 (1993) 432–438. https://doi.org/10.1007/BF02671961.

[23] Q. Gu, Y. Chen, D. Chen, Z. Zhang, Construction of super - hydrophobic copper alloy surface by one - step mixed solution immersion method, IOP Conf. Ser. Earth Environ. Sci. 108 (2018) 022038. https://doi.org/10.1088/1755-1315/108/2/022038.

[24] F.W. Tang, X.Y. Song, H. Bin Wang, X.M. Liu, C. Hou, Thermal Stability of Nanograin Structure in Cu-Zn Alloy System, Defect Diffus. Forum. 381 (2017) 33–38. https://doi.org/10.4028/www.scientific.net/DDF.381.33.

[25] A.P. Lagrow, M.R. Ward, D.C. Lloyd, P.L. Gai, E.D. Boyes, Visualizing the Cu/Cu2O interface transition in nanoparticles with environmental scanning transmission electron microscopy, J. Am. Chem. Soc. 139 (2017) 179–185. https://doi.org/10.1021/jacs.6b08842.

[26] A. Khan, A.P. Patil, T.S. Rao, Effect of zinc addition to copper in improving its corrosion resistance in sulfide polluted synthetic seawater, Trans. Indian Inst. Met. 64 (2011) 99–103. https://doi.org/10.1007/s12666-011-0020-x.

[27] S. Hosseinpour, M. Forslund, C.M. Johnson, J. Pan, C. Leygraf, Atmospheric corrosion of Cu, Zn, and Cu–Zn alloys protected by self-assembled monolayers of alkanethiols, Surf. Sci. 648 (2016) 170–176. https://doi.org/10.1016/j.susc.2015.10.045.

[28] B.J. Kellett, F.F. Lange, Thermodynamics of Densification: I, Sintering of Simple Particle Arrays, Equilibrium Configurations, Pore Stability, and Shrinkage, J. Am.

Ceram. Soc. 72 (1989) 725–734. https://doi.org/10.1111/j.1151-2916.1989.tb06208.x.

[29] C. Chen, K. Suganuma, Microstructure and mechanical properties of sintered Ag particles with flake and spherical shape from nano to micro size, Mater. Des. 162 (2019) 311–321. https://doi.org/10.1016/j.matdes.2018.11.062.

[30] J. Liu, H. Chen, H. Ji, M. Li, Highly Conductive Cu–Cu Joint Formation by Low-Temperature Sintering of Formic Acid-Treated Cu Nanoparticles, ACS Appl. Mater. Interfaces. 8 (2016) 33289–33298. https://doi.org/10.1021/acsami.6b10280.

[31] S.K. Bhogaraju, O. Mokhtari, J. Pascucci, F. Conti, H.R. Kotadia, G. Elger, A multi-pronged approach to low-pressure Cu sintering using surface-modified particles, substrate and chip metallization, in: Int. Symp. Microelectron., 2019: pp. 000387–000392. https://doi.org/10.4071/2380-4505-2019.1.000387.

[32] S. Fu, Y. Mei, X. Li, P. Ning, G.-Q. Lu, Parametric Study on Pressureless Sintering of Nanosilver Paste to Bond Large-Area (≥100 mm2) Power Chips at Low Temperatures for Electronic Packaging, J. Electron. Mater. 44 (2015) 3973–3984. https://doi.org/10.1007/s11664-015-3842-1.

[33] M. Wang, Y. Mei, X. Li, G.Q. Lu, Die-attach on nickel substrate by pressureless sintering a trimodal silver paste, Mater. Lett. 253 (2019) 131–135. https://doi.org/10.1016/j.matlet.2019.06.041.

[34] H. Yan, Y.H. Mei, M. Wang, X. Li, G.Q. Lu, Pressureless sintering multi-scale Ag paste by a commercial vacuum reflowing furnace for massive production of power modules, J. Mater. Sci. Mater. Electron. 30 (2019) 9634–9641. https://doi.org/10.1007/s10854-019-01297-x.

[35] J. Li, X. Li, L. Wang, Y.H. Mei, G.Q. Lu, A novel multiscale silver paste for die bonding on bare copper by low-temperature pressure-free sintering in air, Mater. Des. 140 (2018) 64–72. https://doi.org/10.1016/j.matdes.2017.11.054.

[36] D.B. Butrymowicz, J.R. Manning, M.E. Read, D. Butrymowicz, J.R. Manning, M.E. Read, Diffusion in Copper and Copper Alloys . Part I . Volume and Surface Self - Diffusion in Copper, 643 (2014). https://doi.org/10.1063/1.3253129.